Materials Chemistry and Physics 364 (2026) 132824

Contents lists available at ScienceDirect

Materials Chemistry and Physics

journal homepage: www.elsevier.com/locate/matchemphys

Intrinsic latent heat of the metal-insulator transition in W-doped VO_2

Minsik Kong [a], Sanguk Cho [b], Minsoo An [a], Younghun Jo [c], Dongjin Jang [d], Jong Mok Ok [a,*]

[a] Department of Physics, Pusan National University, Busan, 46241, Republic of Korea
[b] Zero Energy Solution Corp., Gimhae, 50970, Republic of Korea
[c] Research Equipment Development Division, Korea Basic Science Institute, Daejeon, 34113, Republic of Korea
[d] Quantum Magnetic Sensing Group, Korea Research Institute of Standards and Science, Daejeon, 34113, Republic of Korea

HIGHLIGHTS

- W doping lowers VO_2 MIT temperature from ~340 K to ~299 K.
- Volumetric latent heat remains high (237.3 → 161.8 kJ/L).
- Transition entropy decreases from 1.52 to 1.18 k_B/VO_2.
- Higher crystallinity increases entropy change.
- W-doped VO_2 shows near-RT operation with stable latent heat.

ARTICLE INFO

Keywords:
VO_2
Phase-change material
Metal-insulator transition
Latent heat

ABSTRACT

Solid-state phase-change materials (PCMs) are of considerable interest as alternatives to conventional solid-liquid systems because they can provide a thermal response while mitigating issues such as leakage and large volume changes. VO_2 is particularly attractive in this regard because it exhibits a metal-insulator transition (MIT) near room temperature, accompanied by pronounced structural, electrical, magnetic, and thermal changes. Here, we investigate the composition-dependent evolution of the MIT in W-doped VO_2 powders, with particular emphasis on the associated thermodynamic response relevant to functionalities based on a solid-state phase-change. Structural, magnetic, electrical, and thermal properties were characterized by X-ray diffraction, magnetization, electrical resistivity, and differential scanning calorimetry, respectively. The transition temperature decreases systematically from approximately 340 K for undoped VO_2 to about 299 K for the highest-W-content sample (1.239 at%). Despite this substantial suppression of the transition temperature, the volumetric latent heat remains relatively large, decreasing from 237.3 to 161.8 kJ/L, which is higher than those of representative solid-solid PCMs such as NiTi and neopentyl glycol. Meanwhile, the corresponding transition entropy change (ΔS) decreases from 1.52 to 1.18 k_B/VO_2 (from 12.64 to 9.81 J mol^{-1} K^{-1}). Compared with representative phase-change materials, VO_2 occupies a distinctive region that combines near-room-temperature operation and relatively high thermal conductivity, giving rise to the practical advantages of utilizing a solid-state transition. These results demonstrate that W doping enables effective tuning of the MIT temperature while retaining a substantial intrinsic thermodynamic response, underscoring the promise of VO_2 as a viable solid-state phase-change material.

1. Introduction

Phase-change materials (PCMs) have attracted considerable attention for applications in thermal energy storage, thermal management, and caloric devices because they can absorb and release large amounts of heat during phase transitions [1,2]. Conventional PCMs, such as paraffin-based materials and hydrated salts, typically rely on liquid-solid phase transitions and therefore exhibit large latent heats. However, these systems often suffer from intrinsic limitations, including volume expansion, material leakage, phase separation, and degradation during repeated thermal cycling [3,4]. These drawbacks have motivated increasing interest in solid-state phase-transition materials that can

* Corresponding author.
E-mail address: okjongmok@pusan.ac.kr (J.M. Ok).

https://doi.org/10.1016/j.matchemphys.2026.132824
Received 27 April 2026; Received in revised form 11 June 2026; Accepted 17 June 2026
Available online 21 June 2026

provide comparable thermal responses while maintaining structural stability and long-term reliability. Among various candidates, metal-insulator transition (MIT) materials are particularly attractive because their phase transitions occur entirely within the solid state while still producing pronounced changes in electrical, magnetic, structural, and thermal properties. In this class of materials, VO_2 has been one of the most extensively studied systems owing to its sharp first-order transition near room temperature, accompanied by abrupt changes in electrical resistivity, magnetic susceptibility, and crystal structure arising from a coupled electronic and structural phase transition [5–8]. However, the transition temperature of pristine VO_2 is approximately 340 K, which is still higher than room temperature, and suppression of it is mandatory for ubiquitous practical applications. Consequently, numerous studies have focused on tuning the MIT temperature through chemical doping, epitaxial strain, or external stimuli to tailor the functional properties of VO_2 for practical applications such as thermochromic coatings, electrical switching devices, and thermal energy management systems [9–11].

Despite the first-order nature of the MIT in VO_2, comparatively less attention has been paid to the latent heat associated with the transition. Latent heat provides a direct thermodynamic measure of the phase transition, reflecting the entropy change and structural rearrangement involved in the transformation, and is therefore a key parameter governing the thermal functionality of MIT materials when considered as solid-state PCMs. Accordingly, understanding how the latent heat evolves under chemical modification is important not only for clarifying the thermodynamic nature of the transition but also for optimizing the thermal performance of VO_2-based materials [8,12,13].

Although differential scanning calorimetry (DSC) has been widely used to verify the first-order transition in VO_2 and related systems, systematic studies on the evolution of latent heat with W content remain limited [8,14–16]. In particular, the relationship between latent heat and other characteristic signatures of the MIT—such as structural phase evolution and magnetic or electronic responses—has not been clearly established. As a result, it remains unclear whether chemical doping primarily modifies the intrinsic thermodynamic strength of the transition or simply shifts the transition temperature. From a thermodynamic perspective, the transition can be more appropriately described in terms of the transition entropy, ΔS. Depending on the theoretical framework, ΔS has been estimated to be approximately 1.42-1.58 k_B/VO_2, corresponding to a latent heat, Q, of approximately 221.2-246.2 kJ/L (or 11.81-13.14 J mol^{-1} K^{-1}) for $T_c \approx 340$ K [12]. In contrast, experimentally reported powder-based VO_2 samples typically exhibit smaller effective values, reaching only about 198.1 kJ/L for nanoscale VO_2 powders and 208.0 kJ/L for hydrothermally synthesized VO_2 powders [14,16]. This discrepancy suggests that the intrinsic thermodynamic scale of the transition is not fully realized in practical powder samples. In addition, although the first-order nature of the MIT complicates simple analysis, the Mott gap and T_c are strongly correlated and reflect the coupled evolution of electronic and orbital properties. Thus, examining the thermodynamic response together with the transition temperature under W doping may provide additional insight into the evolution of the underlying insulating state.

In this work, we systematically investigate the composition-dependent evolution of the MIT in VO_2 by combining X-ray diffraction (XRD), magnetic and electrical measurements, and differential scanning calorimetry (DSC). Through this multi-probe approach, we quantify the thermodynamic response of the transition, including the latent heat and the corresponding entropy change, and examine its relationship with structural characteristics estimated from the XRD analysis. By showing how the thermodynamic signature of the MIT evolves with W content while retaining a pronounced first-order transition, this study contributes to the understanding of chemically tuned MIT behavior in VO_2 and may inform the development of solid-state phase-change materials based on transition-metal oxides.

2. Experiment details

VO_2 powder was synthesized from V_2O_5 via a solid-state reduction process at 1273 K under an Ar atmosphere. W-doped VO_2 samples were prepared by mixing the synthesized VO_2 powder with WO_3 at different precursor ratios, followed by pelletization and subsequent annealing at 1573 K. The undoped and W-doped samples are hereafter denoted as VW00, VW05, VW10, and VW15, where the numbers indicate nominal W concentrations of 0.0, 0.5, 1.0, and 1.5 at%, respectively. The annealed pellets were reground into fine powders for structural and thermal characterization. The characterization of VO_2 powder was performed using instruments available at the Quantum Matter Core Facility of Pusan National University. Phase identification was performed by X-ray diffraction (XRD, Philips X'Pert^3) using Cu Kα_1 radiation over a 2θ range of 20–80°. Compositional analysis was performed using scanning electron microscopy coupled with energy-dispersive X-ray spectroscopy (SEM-EDS; JEOL JSM-IT800SHL). Thermal properties were examined by differential scanning calorimetry (Discovery DSC 25) in the temperature range of 270–380 K. For electrical and magnetic measurements, the powders were re-pelletized, sealed in evacuated quartz tubes, and annealed at 1273 K for 48 h. Electrical transport and magnetic properties were characterized using a micro-probe system (Nextron MPS-PT) and a Magnetic Property Measurement System (MPMS, QD-USA MPMS3), respectively. Electrical resistivity was measured under a constant current with heating and cooling rates of 3 K/min, and magnetization as a function of temperature was measured over the range of 2–380 K.

3. Results and discussion

The effect of W doping on the crystal structure was examined to clarify the structural evolution associated with the phase transition. Fig. 1 presents the XRD patterns of VW00, VW05, VW10, and VW15 measured at 300 K. As shown in Fig. 1(a), the diffraction patterns of VW00, VW05, and VW10 are dominated by reflections corresponding to the monoclinic M1 phase, whereas additional features associated with the rutile (R) phase become more evident for VW15 [7,11,14]. An enlarged view of the diffraction region near $2\theta \approx 28°$, shown in Fig. 1(b), shows that the M1 (011) reflection shifts systematically toward lower diffraction angles with increasing W content, indicating an increase in the corresponding d-spacing. The calculated d-spacing increases from 3.2007(1) Å for VW00 to 3.2229(1) Å for VW15. This systematic peak shift indicates progressive lattice expansion with W addition, suggesting that W affects the VO_2 crystal lattice rather than merely appearing as an unrelated compositional signal. The detailed structural refinement results are summarized in Fig. S1 and Table S1 of the Supplementary Information. In addition, the gradual decrease in the intensity of the monoclinic reflections suggests a progressive reduction in the M1-phase fraction with increasing W content, consistent with the known tendency of W doping to stabilize the high-temperature rutile-like phase and to lower the transition temperature [11,15,17].

SEM-EDS analysis was performed to evaluate the actual W content of each sample, as summarized in Table 1. The detailed SEM-EDS elemental maps, spectra, and raw compositional analyses are provided in Fig. S2 of the Supplementary Information. The measured cationic W ratios, W/(V + W), were 0.464, 0.833, and 1.239 at% for VW05, VW10, and VW15, respectively. These values are lower than the nominal precursor ratios but increase monotonically with nominal W loading. Therefore, the SEM-EDS-measured W concentrations were used as the composition axis for the quantitative composition-dependent analyses. While SEM-EDS confirms the presence of W and its monotonic increase, it does not provide direct information on the local structural environment of W. Thus, the combined EDS trend, systematic lattice expansion, and monotonic suppression of the MIT temperature are interpreted as mutually consistent evidence for W doping in VO_2.

The magnetic properties across the phase transition were investi-

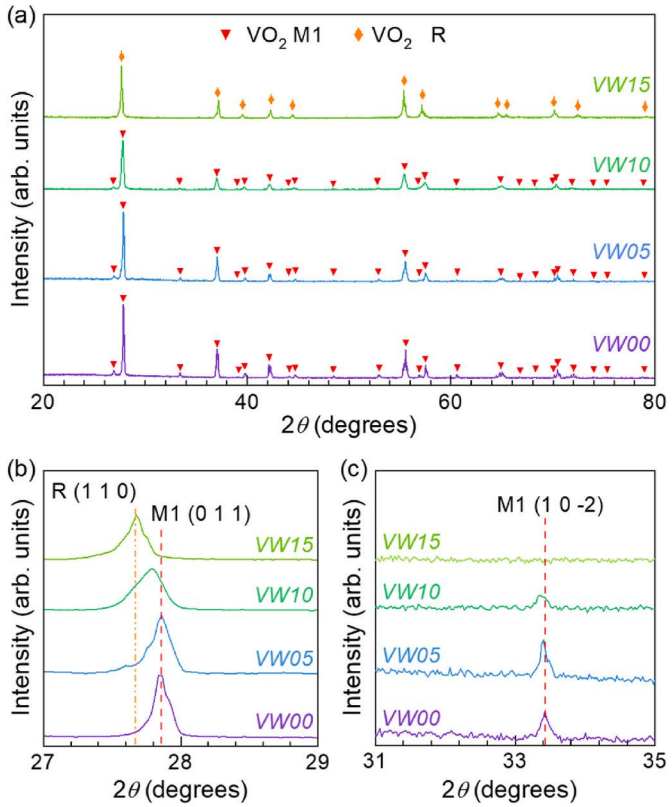

Fig. 1. X-ray diffraction (XRD) patterns of VO_2 samples with different dopant concentrations. (a) Wide-angle XRD patterns showing the diffraction peaks associated with the monoclinic (M1) and rutile (R) phases of VO_2 for the different samples. (b) Enlarged view of the diffraction region near the R (110) and M1 (011) reflections. The dashed lines indicate the reference peak positions of R (110) and M1 (011). (c) Enlarged view of the M1 (1 0 -2) reflection. The dashed lines indicate the reference peak positions.

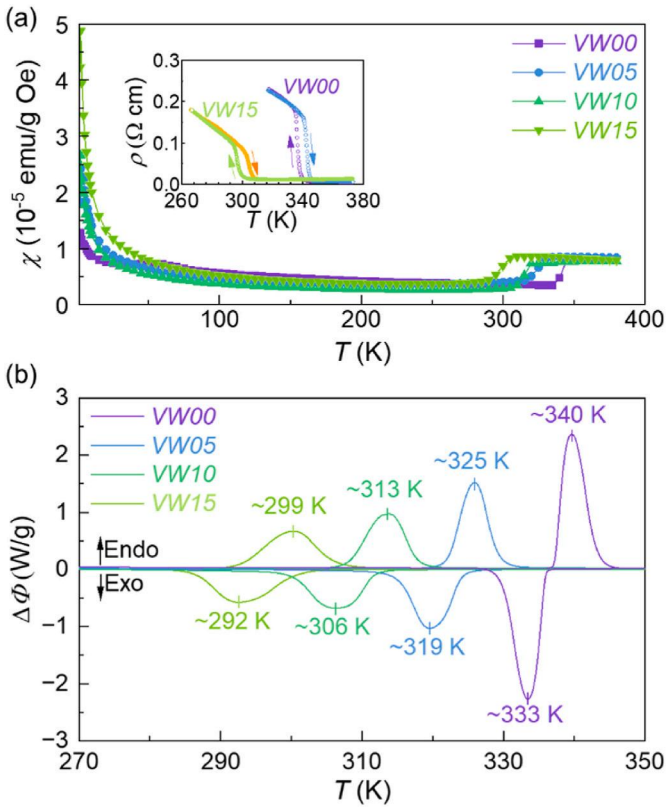

Fig. 2. (a) Temperature dependence of magnetic susceptibility, $\chi(T)$, for VO_2 samples with different W doping concentrations measured under an applied magnetic field. The inset shows the corresponding electrical resistivity, ρ, as a function of temperature, highlighting the metal-insulator transition for each doping level. (b) Differential scanning calorimetry (DSC) curves showing the heat-flow change, $\Delta\Phi$, as a function of temperature for the same samples. The endothermic and exothermic peaks correspond to the phase transitions during heating and cooling, respectively. Different colors indicate different samples, as shown in the legends.

Table 1
Sample IDs and SEM-EDS-measured W concentrations of the VO_2 samples. The sample IDs are based on the nominal precursor ratios, whereas the measured W concentrations were calculated from the cationic ratio W/(V + W) using the SEM-EDS V and W atomic percentages. Detailed elemental maps, spectra, and raw compositional analyses are provided in Fig. S2 of the Supplementary Information.

Sample ID	Nominal W concentration	EDS V at%	EDS W at%	SEM-EDS W content
VW00	0.0 at%	48.9	0.000	0.000 at%
VW05	0.5 at%	46.3	0.216	0.464 at%
VW10	1.0 at%	43.8	0.366	0.833 at%
VW15	1.5 at%	45.7	0.573	1.239 at%

gated by temperature-dependent magnetization measurements using an MPMS. Fig. 2(a) shows the temperature-dependent magnetic susceptibility, $\chi(T)$, for VW00, VW05, VW10, and VW15 measured under a fixed magnetic field. As the temperature increases, all samples exhibit a clear anomaly in the susceptibility curve associated with the MIT. The transition is characterized by a sharp change in $\chi(T)$, near the transition temperature, which systematically shifts toward lower temperatures with increasing W content. Using the SEM-EDS-measured W concentration of 1.239 at% for VW15, this corresponds to a suppression rate of approximately 32 K/at%. The transition temperature was determined from the maximum in the derivative of magnetization with respect to temperature, dM/dT. This trend is in good agreement with previous reports on W-doped VO_2 powders [11,14,15,17]. In addition to the shift in transition temperature, the transition width becomes slightly broader with increasing W content, suggesting a gradual broadening of the phase transformation, likely due to the increased disorder and local lattice distortion associated with W doping. Above the transition temperature, the susceptibility gradually approaches a nearly temperature-independent value on the order of (0.6–0.9) $\times$ 10^{-5} emu·g^{-1}·Oe^{-1}, consistent with a weak paramagnetic response in the metallic phase [6].

At low temperatures, all samples exhibit a pronounced upturn in magnetic susceptibility, forming a divergent tail as the temperature approaches the lowest measured range. The magnitude of this low-temperature tail generally increases with W content. For example, the susceptibility at 2 K increases from approximately 1.3 $\times$ 10^{-5} emu·g^{-1}·Oe^{-1} for VW00 to about 4.8 $\times$ 10^{-5} emu·g^{-1}·Oe^{-1} for VW15, corresponding to an enhancement by a factor of about 3.8. Such a Curie-like upturn likely originates from localized paramagnetic moments associated with defects or doping-induced electronic inhomogeneity, rather than from the intrinsic magnetic response of the VO_2 lattice [18]. A Curie–Weiss analysis of the low-temperature susceptibility (20–120 K) was performed to quantify the Curie-like magnetic response, with representative fitting curves and extracted fitting parameters provided in Supplementary Fig. S3 and Table S2. For the W-doped samples, the extracted effective magnetic moment remains in the range of 0.39–0.46 μ_B/V. This magnitude is qualitatively consistent with localized V-related magnetic moments generated by W-induced charge compensation and defect/electronic inhomogeneity, rather than isolated W-centered moments alone. Representative M − H curves are provided in Fig. S4 of the

Supplementary Information, showing the overall weak paramagnetic response across the measured temperature range.

To complement the magnetic susceptibility measurements and to provide an independent confirmation of the metal–insulator transition, representative electrical resistivity data are shown in the inset of Fig. 2 (a) for VW00 and VW15. Reliable resistivity measurements on pelletized polycrystalline powder samples are experimentally challenging because of grain-boundary effects, interparticle contact resistance, and sample inhomogeneity. Intermediate compositions showed limited reproducibility during thermal cycling, preventing reliable quantitative comparison across the full composition series. Therefore, the composition-dependent evolution of the transition temperature was primarily evaluated from the magnetic susceptibility data. For both compositions, the resistivity exhibits an abrupt change of approximately one order of magnitude upon heating, confirming the occurrence of a well-defined MIT. Although the magnitude of the resistivity change is smaller than that typically reported for dense thin films or single crystals, this reduced contrast is reasonably attributed to the polycrystalline powder nature of the samples and the associated extrinsic transport contributions. Nevertheless, the sharp resistivity drops, and clear thermal hysteresis still demonstrate the first-order character of the transition. The resistivity decreases sharply from about 10^{-1} Ω cm in the insulating phase to approximately 10^{-2} Ω cm in the metallic phase. Compared with VW00, the transition in VW15 occurs at a significantly lower temperature, shifting from approximately 342 K to 304 K, corresponding to a reduction of about 38 K. The transition width, estimated from the temperature range over which the resistivity changes most rapidly, is approximately 5.7 K for VW00 and slightly broader for VW15 (7.2 K), indicating a gradual broadening of the transition with W addition. Although resistivity measurements were performed only for these two representative compositions, the observed behavior is consistent with the composition-dependent shift of the MIT temperature identified from the magnetization measurements. This agreement between the electrical and magnetic responses supports the interpretation that the anomalies observed in the magnetization curves originate from the MIT rather than from extrinsic magnetic effects.

Finally, the thermal response associated with the phase transition was examined by DSC. Fig. 2(b) shows the DSC curves measured during heating and cooling for VW00, VW05, VW10, and VW15. All samples exhibit well-defined endothermic and exothermic peaks, confirming the first-order nature of the phase transition. Upon heating, the transition temperature systematically shifts toward lower temperatures with increasing W content, decreasing from 340 K for VW00 to 299 K for VW15. During cooling, the corresponding transition temperatures are observed at 333 K and 292 K, respectively. The thermal hysteresis remains within a narrow range of approximately 6–7 K across all samples, indicating that W doping does not significantly affect the thermal reversibility of the phase transition. This preserved hysteresis further reinforces the first-order character of the transition across the entire composition series. The latent heat Q decreases from 237.3 kJ/L for VW00 to 161.8 kJ/L for VW15, while remaining relatively large and comparable to values reported previously for W-doped VO_2 powders [14,15,17,19].

For comparison, the transition temperatures obtained in this work were compared with previously reported values for W-doped VO_2, as summarized in Fig. 3(a). For the present samples, the W concentrations were plotted using the SEM–EDS-measured cationic ratios, W/(V + W), whereas the literature data were plotted using the concentrations reported in the original references. The transition temperatures determined from both MPMS and DSC measurements follow the same monotonic decreasing trend with increasing W content reported in the literature [11,15,17,20]. A linear fit to the present data using the SEM-EDS-measured W concentrations yields a transition-temperature suppression rate of approximately −33 K/at%, which lies at the upper end of the reported range and indicates a relatively strong sensitivity of the phase transition to W doping [11,15,17,20]. This comparison

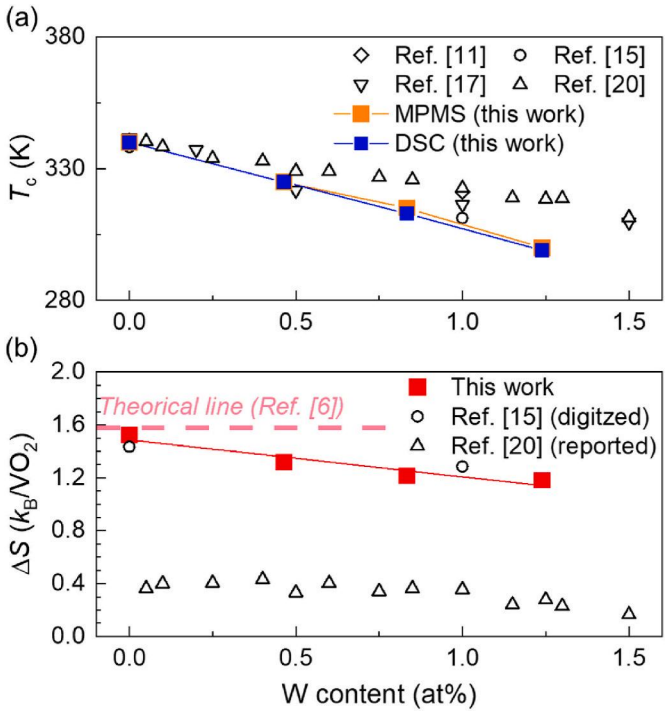

Fig. 3. (a) Transition temperature T_c of W-doped VO_2 as a function of W concentration. The values obtained from MPMS (orange squares) and DSC (blue squares) in this work are compared with literature data (open symbols): diamonds [11], circles [15], inverted triangles [17], and triangles [20]. For the present data, the W contents correspond to the SEM-EDS-measured cationic ratios, W/(V + W), whereas the literature data are plotted using the concentrations reported in the original references. (b) Transition entropy change, ΔS, as a function of W concentration. The present data (red squares) are compared with literature values from Ref. [15] (open circles, digitized) and Ref. [20] (open triangles, reported). The red solid line is a linear fit to the present data, and the pink dashed line represents the theoretical value from Ref. [6].

demonstrates that the present samples exhibit a pronounced reduction in transition temperature while remaining consistent with established trends. Fig. 3(b) focuses on the thermodynamic response associated with the phase transition in terms of the transition entropy, $\Delta S = Q/T_c$. The estimated entropy changes decrease systematically from 1.52 to 1.18 k_B/VO_2 (from 12.64 to 9.81 J mol^{-1} K^{-1}) as the SEM–EDS-measured W concentration increases from 0 to 1.239 at%, with intermediate values of 1.32 and 1.22 k_B/VO_2 (10.94 and 10.14 J mol^{-1} K^{-1}) for VW05 and VW10, respectively. A linear fit to the present ΔS data using the measured W concentrations gives a slope of approximately −0.277 k_B/VO_2 per at%, corresponding to −2.30 J mol^{-1} K^{-1} per at%. These values remain significantly higher than the reported values in Ref. [20] over a comparable composition range and are also slightly higher than the values from Ref. [15]. Notably, the entropy of VW00 is close to the theoretical estimate of 1.58 k_B/VO_2 (13.14 J mol^{-1} K^{-1}) indicated in Fig. 3(b) [6]. In contrast, the entropy decreases moderately with W content, indicating that the reduction in latent heat cannot be explained solely by the suppression of T_c. Since $\Delta S = Q/T_c$, the stronger decrease in latent heat than in T_c suggests that the phase transition becomes progressively less thermodynamically abrupt with increasing W content, resulting in a reduced amount of heat exchanged per unit temperature at the transition point. Nevertheless, the relatively high transition entropy together with the strong tunability of the transition temperature supports the potential of W-doped VO_2 as a competitive solid-state PCM.

To further examine the role of structural quality in the phase-transition thermodynamics, the measured entropy change was compared with the relative crystallinity estimated from the XRD analysis, as shown in Fig. 4(a). The samples labeled S1–S5 in Fig. 4(a) denote

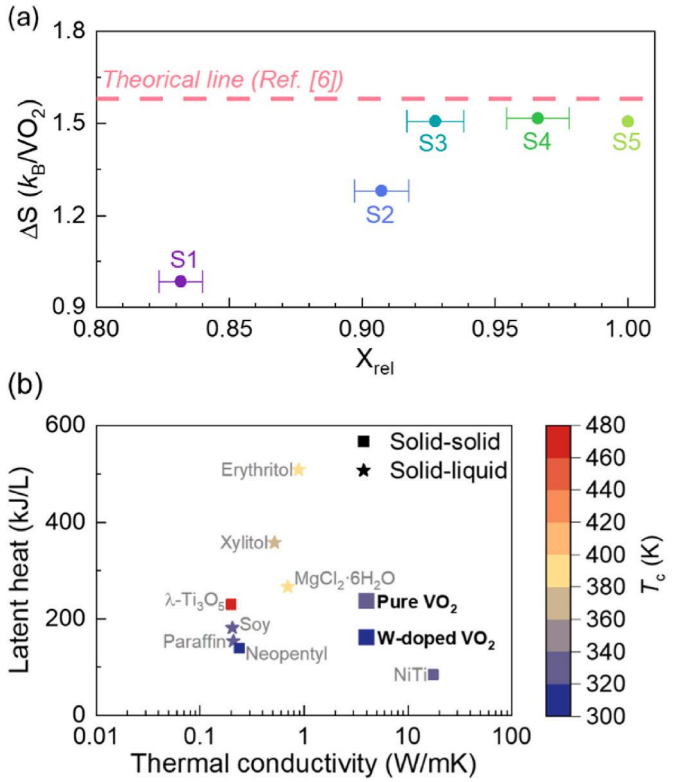

Fig. 4. (a) Entropy change, ΔS, plotted as a function of the relative crystallinity. The dashed line indicates the theoretical reference value. (b) Literature-based comparison of volumetric latent heat and thermal conductivity for representative phase-change materials, including both solid-solid and solid-liquid systems. Squares and stars denote solid-solid and solid-liquid materials, respectively, and the color scale indicates the phase-transition temperature, T_c. The VO_2-based samples investigated in the present work are indicated as VO_2 and W-VO_2, where W-VO_2 corresponds to the highest-W-content sample. Literature data for paraffin wax, soy, xylitol, erythritol, $MgCl_2{\cdot}6H_2O$, neopentyl glycol, NiTi, and λ-Ti_3O_5 were taken from Refs. [22–26]. For VO_2, the volumetric latent heat values were obtained in the present work, whereas the thermal conductivity values were adopted from previously reported literature data for pelletized VO_2 powders [27].

undoped VO_2 specimens prepared under different conditions and used here to examine sample-to-sample variations in crystalline quality. Although all these samples are compositionally undoped VO_2, slight variations in the transition temperature were still observed among them. For this reason, the entropy change ΔS was used for comparison to reduce the influence of the sample-to-sample variation in transition temperature. The relative crystallinity, X_{rel}, was evaluated from the XRD patterns based on the ratio between the crystalline diffraction peaks and the amorphous background. Because the background level can vary depending on the measurement setup, a reliable absolute quantification is difficult, whereas relative comparisons within the same measurement conditions remain robust. Therefore, the sample exhibiting the highest peak-area ratio was taken as a reference ($X_{rel} = 1$), and the relative crystallinity of the other samples was determined accordingly. The corresponding uncertainties were estimated from the baseline variation and propagated through the normalization procedure. The detailed procedure used to determine X_{rel} and its uncertainty is provided in Fig. S5 of the Supplementary Information. As shown in Fig. 4(a), ΔS increases with increasing X_{rel}, showing a proportional dependence at lower crystallinity and a tendency toward saturation at higher crystallinity. Samples with larger relative crystallinity generally exhibit values of ΔS closer to the theoretical value indicated by the dashed line. This behavior suggests that improved crystalline quality helps preserve the entropy change associated with the metal-insulator transition. In this context, a lower X_{rel} may reflect increased microstructural disorder, such as smaller coherently ordered domains, local strain, defect-rich regions, or a larger noncrystalline background contribution, which can broaden the transition and reduce the fraction of the sample participating cooperatively in the first-order MIT. Consistent with this interpretation, previous studies have shown that post-annealing can partially recover the phase-transition thermodynamics of VO_2 by improving crystalline quality and relieving microstructural disorder [19,21]. These results suggest that crystalline quality is an important factor in determining the magnitude of the transition entropy change, even when the chemical composition is unchanged. The rutile-phase fraction observed at room temperature in the higher W-content samples may also influence the measured latent heat and transition entropy, since the XRD measurements may have been performed within the phase-transition region where M1/R coexistence can occur. Therefore, the reductions in Q and ΔS should be interpreted with consideration of both intrinsic thermodynamic changes associated with W addition and possible room-temperature phase coexistence.

Fig. 4(b) presents a literature-based comparison of volumetric latent heat and thermal conductivity among representative phase-change materials, where the latent heat values for VO_2 are obtained in the present work and the thermal conductivity values are adopted from previously reported data [27]. The comparison includes conventional organic and salt-hydrate PCMs such as paraffin wax, xylitol, erythritol, and $MgCl_2{\cdot}6H_2O$, as well as representative solid-solid systems including neopentyl glycol, NiTi, and λ-Ti_3O_5 [22–24]. Within this comparative framework, VO_2 appears to occupy a distinctive regime characterized by relatively high volumetric latent heat among solid-solid PCMs, exceeding representative materials such as neopentyl glycol and NiTi, while remaining comparable to conventional solid-liquid PCMs and exhibiting higher thermal conductivity than most organic and salt-hydrate PCMs [22–25]. Although their latent heat is lower than some of solid-liquid PCMs, VO_2 retains the intrinsic advantages of a solid-solid phase transition, including the absence of leakage and improved structural stability [28,29]. In addition, the transition temperature of the W-containing VO_2 samples investigated here remains close to room temperature. Taken together, these literature-based comparisons suggest that VO_2 is a promising PCM candidate, combining near-room-temperature operation, relatively high thermal conductivity, and the inherent advantages of solid-state reversibility.

4. Conclusion

In summary, we systematically investigated the effect of W content on the structural, magnetic, electrical, and thermal properties of VO_2 powders, with particular emphasis on the thermodynamic response associated with the metal-insulator transition. XRD measurements show that the monoclinic VO_2 phase is preserved in VW00, VW05, and VW10, while a rutile phase emerges in VW15, accompanied by lattice expansion. Magnetization and electrical resistivity measurements reveal a systematic suppression of the transition temperature with increasing W content, from approximately 340 K for VW00 to 299 K for VW15, while differential scanning calorimetry confirms the persistence of a clear first-order phase transition. Despite the substantial reduction in transition temperature, the volumetric latent heat remains relatively large, and the corresponding entropy change (ΔS) indicates that W addition reduces not only T_c but also the intrinsic thermodynamic driving force of the transition. Furthermore, ΔS increases with increasing relative crystallinity, suggesting that crystalline quality plays a key role in preserving the intrinsic thermodynamic response.

Taken together, these results demonstrate that VO_2 combines tunable transition temperature with a substantial thermodynamic response, placing it in a distinctive regime among phase-change materials. In particular, the VO_2-based samples exhibit relatively high latent heat values among solid-solid systems, values comparable to those of some solid-liquid PCMs, and the intrinsic advantages of solid-state

reversibility. These findings establish W-containing VO_2 as a viable solid-state phase-change material and highlight the importance of simultaneously controlling chemical composition and crystalline quality for optimizing its thermal functionality.

CRediT authorship contribution statement

Minsik Kong: Writing – review & editing, Writing – original draft, Investigation, Formal analysis, Conceptualization. **Sanguk Cho:** Writing – review & editing, Investigation. **Minsoo An:** Writing – review & editing, Investigation. **Younghun Jo:** Writing – review & editing, Investigation. **Dongjin Jang:** Writing – review & editing, Investigation. **Jong Mok Ok:** Writing – review & editing, Writing – original draft, Supervision, Investigation, Conceptualization.

Declaration of competing interest

The authors declare that they have no known competing financial interests or personal relationships that could have appeared to influence the work reported in this paper.

Acknowledgements

This work was supported by the National Research Foundation of Korea (NRF) grant funded by the Korea government (MSIT) (RS-2023-00210295, RS-2023-00281839, RS-2025-25453111).

Supporting Information

Supporting Information is available from the author.

Appendix A. Supplementary data

Supplementary data to this article can be found online at https://doi.org/10.1016/j.matchemphys.2026.132824.

Data availability

Data will be made available on request.

References

[1] A. Sharma, V.V. Tyagi, C.R. Chen, D. Buddhi, Review on thermal energy storage with phase change materials and applications, Renew. Sustain. Energy Rev. 13 (2009) 318–345, https://doi.org/10.1016/j.rser.2007.10.005.
[2] M. Kenisarin, K. Mahkamov, Solar energy storage using phase change materials, Renew. Sustain. Energy Rev. 11 (2007) 1913–1965, https://doi.org/10.1016/j.rser.2006.05.005.
[3] A. Anand, A. Shukla, A. Kumar, D. Buddhi, A. Sharma, Cycle test stability and corrosion evaluation of phase change materials used in thermal energy storage systems, J. Energy Storage 39 (2021), https://doi.org/10.1016/j.est.2021.102664.
[4] G. Ferrer, A. Solé, C. Barreneche, I. Martorell, L.F. Cabeza, Review on the methodology used in thermal stability characterization of phase change materials, Renew. Sustain. Energy Rev. 50 (2015) 665–685, https://doi.org/10.1016/j.rser.2015.04.187.
[5] F.J. Morin, Oxides which show a metal-to-insulator transition at the neel temperature, Phys. Rev. Lett. 3 (1959) 34–36, https://doi.org/10.1103/PhysRevLett.3.34.
[6] C.N. Berglund, H.J. Guggenheim, Electronic properties of VO_2 near the semiconductor-metal transition, Phys. Rev. 185 (1969) 1022–1033, https://doi.org/10.1103/PhysRev.185.1022.
[7] J.B. Goodenough, The two components of the crystallographic transition in VO_2, J. Solid State Chem. 3 (1971) 490–500, https://doi.org/10.1016/0022-4596(71)90091-0.
[8] K. Kato, J. Lee, A. Fujita, T. Shirai, Y. Kinemuchi, Influence of strain on latent heat of VO_2 ceramics, J. Alloys Compd. 751 (2018) 241–246, https://doi.org/10.1016/j.jallcom.2018.04.094.
[9] Y. Muraoka, Z. Hiroi, Metal–insulator transition of VO_2 thin films grown on TiO_2 (001) and (110) substrates, Appl. Phys. Lett. 80 (2002) 583–585, https://doi.org/10.1063/1.1446215.
[10] J. Jeong, N. Aetukuri, T. Graf, T.D. Schladt, M.G. Samant, S.S. Parkin, Suppression of metal-insulator transition in VO_2 by electric field-induced oxygen vacancy formation, Science 339 (2013) 1402–1405, https://doi.org/10.1126/science.1230512.
[11] Z.F. Peng, Y. Wang, Y.Y. Du, D. Lu, D.Z. Sun, Phase transition and IR properties of tungsten-doped vanadium dioxide nanopowders, J. Alloys Compd. 480 (2009) 537–540, https://doi.org/10.1016/j.jallcom.2009.01.092.
[12] T.A. Mellan, H. Wang, U. Schwingenschlögl, R. Grau-Crespo, Origin of the transition entropy in vanadium dioxide, Phys. Rev. B 99 (2019) 064113, https://doi.org/10.1103/PhysRevB.99.064113.
[13] M. Wang, Y. Xue, Z. Cui, R. Zhang, Size-dependent crystal transition thermodynamics of Nano-VO_2 (M), J. Phys. Chem. C 122 (2018) 8621–8627, https://doi.org/10.1021/acs.jpcc.8b01183.
[14] F.Y. Kong, M. Li, S.S. Pan, Y.X. Zhang, G.H. Li, Synthesis and thermal stability of W-doped VO_2 nanocrystals, Mater. Res. Bull. 46 (2011) 2100–2104, https://doi.org/10.1016/j.materresbull.2011.06.030.
[15] J. Zou, H. Shi, X. Su, Q. Feng, S. Liang, A simple method to prepare $V_{1-x}W_xO_2$ (x = 0, 0.01, 0.02, 0.03, 0.04, and 0.05) controllable phase transition temperature powder, J. Alloys Compd. 708 (2017) 706–712, https://doi.org/10.1016/j.jallcom.2017.03.081.
[16] M. Van Zele, H. Rijckaert, L.V. Bossele, D. Deduytsche, L. Van Daele, E. Drijvers, C. Detavernier, I. Van Driessche, K. De Buysser, Microwave-assisted synthesis of nanoscale VO_2 structures, Open Ceram. 7 (2021) 100155, https://doi.org/10.1016/j.oceram.2021.100155.
[17] Y.B. Xue, T. Sekino, L. Miao, T. Hasegawa, A. Okawa, T. Goto, S. Yin, Y. Seo, Insights into the phase transition behavior of thermochromic VO_2 (M1) powders doped with Tungsten, Adv. Powder Technol. 36 (2025) 104857, https://doi.org/10.1016/j.apt.2025.104857.
[18] D. Paquet, P. Leroux-Hugon, Electron correlations and electron-lattice interactions in the metal-insulator, ferro-elastic transition in VO_2: a thermodynamical study, Phys. Rev. B 22 (1980) 5284–5301, https://doi.org/10.1103/PhysRevB.22.5284.
[19] J. Zou, X. Chen, L. Xiao, Phase transition performance recovery of W-doped VO_2 by annealing treatment, Mater. Res. Express 5 (2018) 065055, https://doi.org/10.1088/2053-1591/aacd8c.
[20] F.M. Morales, M. Escanciano, M.P. Yeste, A.J. Santos, Reactivity of vanadium nanoparticles with oxygen and tungsten, Nanomaterials 12 (2022) 1471, https://doi.org/10.3390/nano12091471.
[21] K.L. Gurunatha, S. Sathasivam, J. Li, M. Portnoi, I.P. Parkin, I. Papakonstantinou, Combined effect of temperature induced strain and oxygen vacancy on metal-insulator transition of VO_2 colloidal particles, Adv. Funct. Mater. 30 (2020) 2005311, https://doi.org/10.1002/adfm.202005311.
[22] S. Hohlein, A. Konig-Haagen, D. Bruggemann, Thermophysical characterization of $MgCl_2 \bullet 6H_2O$, Xylitol and Erythritol as Phase Change Materials (PCM) for Latent Heat Thermal Energy Storage (LHTES), Materials (Basel) 10 (2017) 444, https://doi.org/10.3390/ma10040444.
[23] D.J. Sharar, B.F. Donovan, R.J. Warzoha, A.A. Wilson, A.C. Leff, B.M. Hanrahan, Solid-state thermal energy storage using reversible martensitic transformations, Appl. Phys. Lett. 114 (2019) 143902, https://doi.org/10.1063/1.5087135.
[24] H. Tokoro, M. Yoshikiyo, K. Imoto, A. Namai, T. Nasu, K. Nakagawa, N. Ozaki, F. Hakoe, K. Tanaka, K. Chiba, R. Makiura, K. Prassides, S. Ohkoshi, External stimulation-controllable heat-storage ceramics, Nat. Commun. 6 (2015) 7037, https://doi.org/10.1038/ncomms8037.
[25] A.P. Singh, S. Khanna, S. Paneliya, H. Hinsu, Y. Patel, B. Mehta, Preparation and characterization of solid-state neopentyl glycol/expanded graphite micro composite for thermal energy storage applications, Mater. Today Proc. 47 (2021) 621–625, https://doi.org/10.1016/j.matpr.2020.11.403.
[26] D.K. Yadav, P.K.S. Rathore, R.K. Singh, A.K. Gupta, B.S. Sikarwar, Experimental Study on paraffin wax and Soya wax supported by high-density polyethylene and loaded with nano-additives for thermal energy storage, Energies 17 (2024) 2461, https://doi.org/10.3390/en17112461.
[27] C.L. Gomez-Heredia, J.A. Ramirez-Rincon, D. Bhardwaj, P. Rajasekar, I.J. Tadeo, J. L. Cervantes-Lopez, J. Ordonez-Miranda, O. Ares, A.M. Umarji, J. Drevillon, K. Joulain, Y. Ezzahri, J.J. Alvarado-Gil, Measurement of the hysteretic thermal properties of W-doped and undoped nanocrystalline powders of VO_2, Sci. Rep. 9 (2019) 14687, https://doi.org/10.1038/s41598-019-51162-4.
[28] A. Fallahi, G. Guldentops, M.J. Tao, S. Granados-Focil, S. Van Dessel, Review on solid-solid phase change materials for thermal energy storage: molecular structure and thermal properties, Appl. Therm. Eng. 127 (2017) 1427–1441, https://doi.org/10.1016/j.applthermaleng.2017.08.161.
[29] M.Y. Zhi, S. Yue, L.L. Zheng, B.J. Su, J. Fu, Q. Sun, Recent developments in solid-solid phase change materials for thermal energy storage applications, J. Energy Storage 89 (2024) 111570, https://doi.org/10.1016/j.est.2024.111570.